frontiers | Frontiers in Astronomy and Space Sciences

TYPE Original Research
PUBLISHED 21 August 2025
DOI 10.3389/fspas.2025.1633524

OPEN ACCESS

EDITED BY
Orenthal Tucker,
NASA Goddard Space Flight Center,
United States

REVIEWED BY
Shican Qiu,
Chang'an University, China
Sarah Henderson,
The University of Iowa, United States

*CORRESPONDENCE
Dmitry Bisikalo,
bisikalo@inasan.ru

RECEIVED 22 May 2025
ACCEPTED 17 July 2025
PUBLISHED 21 August 2025

CITATION
Shematovich V and Bisikalo D (2025) Modeling of non-thermal fractions formed in the extended hydrogen corona at Mars. *Front. Astron. Space Sci.* 12:1633524. doi: 10.3389/fspas.2025.1633524

Modeling of non-thermal fractions formed in the extended hydrogen corona at Mars

Valery Shematovich[1] and Dmitry Bisikalo[1,2]*

[1]Institute of Astronomy, Russian Academy of Sciences, Moscow, Russia, [2]National Centre of Physics and Mathematics, Moscow, Russia

Solar forcing on the upper atmospheres of terrestrial planets occurs through both the absorption of soft X-ray and extreme ultraviolet (XUV) solar radiation and the influx of solar wind plasma resulting in the formation of an extended neutral corona populated by suprathermal (hot) H, C, N and O atoms. Observations by the Imaging UV Spectrograph (IUVS) onboard of the Mars Atmosphere and Volatile EvolutioN (MAVEN) space mission at Mars confirmed the presence of an extended corona containing both thermal and suprathermal (formally with kinetic energies below 10 eV) fractions of hydrogen, carbon, and oxygen atoms. The solar wind influx also produces super-thermal atoms—energetic neutral atoms (ENAs; kinetic energies >10 eV)—via charge exchange between high-energy solar wind protons and coronal thermal neutrals. These ENAs transfer solar wind energy into the Martian neutral atmosphere. Notably, this charge-exchange process serves as an active aeronomic mechanism for generating supra- and super-thermal hydrogen populations in Mars' extended corona and may act as a potential driver for similar phenomena on other planets. The spatial and energy distributions of both non-thermal atomic hydrogen populations in the Martian extended corona were computed using kinetic Monte Carlo models. These non-thermal H fractions must be considered when interpreting remote observations of planetary coronae. Our calculations reveal that non-thermal escape rates can reach ~26% of the thermal escape rate during aphelion and solar minimum conditions. This finding has significant implications for Mars' atmospheric evolution: while current escape rates are modulated by solar activity, the more active young Sun likely drove substantially higher non-thermal escape. This mechanism may have played a key role in Mars' long-term water loss.

KEYWORDS

extended planetary corona, solar wind, charge exchange, suprathermal atoms, UV observations, kinetic modeling

1 Introduction

Terrestrial planets lose a certain amount of their atmospheres every day due to solar-terrestrial interactions. The exosphere (or corona) of a planet connects its near-surface atmosphere with interplanetary space and contains key information about the mechanism of this loss. This region is mostly filled with neutral hydrogen atoms, which resonantly scatter solar Ly-α photons, creating a global glow phenomenon called a planetary corona. Usually, above several radii of a terrestrial planet, the exosphere is in an optically thin

state, so the measurement of the Ly-α radiation integral over the line of sight shows a linear dependence on the local radial density in the exosphere. This is used to construct models of the H density in the exosphere based on measurements of the Ly-α luminosity. Studying the density of thermal and hot fractions of hydrogen atoms in the planetary corona and the reaction to various space conditions is the key to understanding the past, present, and future of the atmosphere of terrestrial-type planets and to conclusions about the evolution of their atmospheres both in the Solar System and in planetary systems of other stars.

The loss of the planetary atmosphere (or atmospheric escape) due to thermal and non-thermal processes plays an important role in the evolution of planetary atmospheres, primarily, of terrestrial planets in the Solar System, although many details of this phenomenon remain unclear and continue to be actively discussed (Brain et al., 2017; Chaufray et al., 2024; Kleinboehl et al., 2024; Yelle, 2024). Note that for atmospheric loss due to the escape of neutral atoms and molecules, there is no direct measurements of escape fluxes, and to estimate the loss rate of a neutral planetary atmosphere, it is necessary to develop mathematical models for this class of aeronomic problems (Johnson et al., 2008; Shematovich and Marov, 2018; Bisikalo et al., 2021).

The loss of Martian atmosphere has profound implications for both astrobiology and planetary evolution, reshaping our understanding of habitability, climate dynamics, and the potential for life beyond Earth (Jakosky et al., 2018; Jakosky, 2021). The atmospheric loss led to a drop in pressure and temperature, preventing stable liquid water - a key requirement for life, as we know it - from existing on the surface for prolonged periods (Jakosky, 2024; Jakosky and Hallis, 2024). Mars exemplifies how planetary size (lower gravity), magnetic fields, and stellar proximity affect atmospheric retention and, therefore, may represent a common planetary outcome-worlds that started Earth-like but lost habitability due to atmospheric escape (see, for example, Tian, 2015; Tian et al., 2018; Bergstern et al., 2024). Martian atmospheric loss turned it from a potentially habitable world into a frigid desert, but its history offers a template for studying planetary habitability's fragility (Cockell et al., 2016). For astrobiology and planetary evolution, it underscores the need to search for life in subsurface or extinct environments, and highlights the delicate balance required to sustain atmospheres.

At present, quite effective numerical models have been developed to predict the thermal fractions of hydrogen atoms in the coronae of terrestrial planets (see, for example, Baliukin et al., 2019; Chaffin et al., 2021; Clarke et al., 2024), which in general use the analytic representation (Chamberlain, 1963) of the planetary exosphere. On the other hand, the interpretation of observations of solar radiation scattering in the hydrogen HI Ly-α line indicates the need to involve both thermal and non-thermal (hot) fraction of atomic hydrogen in extended hydrogen coronae for Venus, Earth, and Mars (see, e.g., Nagy et al., 1990; Qin, and Waldrop, 2016; Bhattacharyya et al., 2023).

The history of Mars is assumed to have had a dense, warm, and humid atmosphere at the turn of the so-called Noachian and Hesperian epochs (~4–3.6 billion years ago), preceding the modern Amazonian epoch of cold and dry Mars (Carr and Head, 2003). In order for early Mars to be warm and humid, it is assumed that it had a dense CO_2 atmosphere (Kasting, 1988). Recent studies (Wordsworth et al., 2017) show that the addition of even a small amount of methane (the second most effective greenhouse gas after CO_2) to a thin carbon dioxide atmosphere leads to a sharp increase in the greenhouse effect, raising the temperature by tens of degrees Kelvin with an increase in the CH_4 concentration of only one percent. In other words, if the early atmosphere of Mars was as dense as the atmosphere of Earth, the surface temperature of Mars would be similar to that of modern Earth with a methane concentration of only two to 10 percent. Since Mars is only one-tenth the mass of Earth, it would hardly be capable of having a CO_2 atmosphere with a pressure of more than 1 bar in the early Noachian epoch (Tian, 2015). Meanwhile, a favorable factor for maintaining a sufficiently dense atmosphere could have been the fact that atmospheric loss from Mars during the Noachian-Hesperian epochs with low solar luminosity was relatively small (Tian, 2015; Jakosky, 2021; 2024).

Current space and surface studies at Mars indicate that planet's surface had copious liquid water early in its evolutionary history. Geological estimates and surface Deuterium/Hydrogen ratio (D/H) mapping put the total amount of water lost by Mars anywhere between 100–1,500 m of Global Equivalent Layer (GEL) (Carr and Head, 2003; Mahaffy et al., 2015; Villanueva et al., 2015). Remote sensing, which tracks atmospheric water vapor losses by observing hydrogen escape, on the other hand, puts the total water loss estimate only at 23 m of GEL (Jakosky et al., 2018), resulting in a large discrepancy with the surface values. One of the reasons for this disparity is likely because remoting sensing estimates are made exclusively by extrapolating the present-day escape rate of thermal H atoms back in time. These escape rates are estimated purely from the photodissociation of water vapor (Hunten and McElroy, 1970; McElroy and Donahue, 1972) and do not account for escaping non-thermal H atoms (Jakosky et al., 2018; Bhattacharyya et al., 2023).

The extended exosphere of Mars was first discovered by Mariner 6 and 7 in the late 1960s and early 1970s through observations of solar Ly-α photons resonantly scattered by H atoms in the exosphere (Barth et al., 1969; Barth et al., 1970; Anderson Jr and Hord, 1971; Anderson Jr, 1974). Since then, the study of the Martian exosphere has advanced significantly using the same remote sensing technique. Analysis of the Ly-α emission line observed in the far ultraviolet by the Hubble Space Telescope HST) and Mars Expres (MEX) has reveald an order-of-magnitude change in the H escape heat flux during the dust storm sea (Clarke et al., 2014; Chaffin et al., 2014; Bhattacharyya et al., 2015). It is worth oting that the escape rate peak was also detected in measurements onboard MAVEN spacecraft, which significantly extended the observational chronology by several Martian years (Clarke et al., 2017; Clarke et al., 024; Halekas, 2017; Chaffin et al., 2018; Mayyasi et al., 2019). Despite all these discoveries, it was not possible to confirm in observations the presence of energetic non-thermal hydrogen atoms in the Martian exosphere.

The first proxy for non-thermal H on Mars was obtained from the analysis of MEX observations of Ly-α emission in the Martian exosphere (Chaufray et al., 2007; Chaufray et al., 2008; Chaffin et al., 2014). Well-chosen temperature limits (~170–350 K) for thermal H atoms determined from thermospheric observations and global circulation models (GCMs) (see, e.g., Bougher et al., 2017) could not match the Ly-α intensity profiles measured by MEX. Instead, significantly higher temperatures (>350 K) were required to approximate the observed emission intensities. The same

situation was found by HST observations of the Martian exosphere (Clarke et al., 2014; Bhattacharyya et al., 2015; Bhattacharyya et al., 2017a; Bhattacharyya et al., 2017b). Attempts to spectrally separate the energetic population from the dominant thermal H atoms did not yield any positive results, since the temperature difference between them was not large enough to be observed as a detectable Doppler-shifted signal at the resolution of available instruments. Another possibility to detect energetic non-thermal H was to discern a change in the slope of the Ly-α intensity profile as the exosphere transitioned from being dominated by the thermal H fraction at altitudes slightly above the exobase to being dominated by the non-thermal H fraction at higher altitudes. Similar changes in the Ly-α intensity profile with altitude have been observed on Venus and Earth (Chaufray et al., 2012; Carruthers et al., 1976).

The numeric study of the formation and loss for non-thermal fractions of hydrogen atoms described in this paper is highly relevant, since the NASA MAVEN spacecraft is currently located in the atmosphere of Mars, aimed at studying the processes of atmosphere loss. It seems that the loss of the neutral atmosphere of Mars due to the precipitating fluxes of protons and hydrogen atoms with high energies during solar flares may become the dominant process of atmosphere loss on Mars on geological time scales (Jakosky et al., 2018; Bhattacharyya et al., 2023). Moreover, understanding the contribution of non-thermal H to the escape rate is important for determining the actual present-day escape rate of water from the Martian exosphere. A prior study found that the contribution of the suprathermal H fraction is significant and cannot be neglected (Bhattacharyya et al., 2023). Accordingly, it becomes possible to compare the results of calculations of the H non-thermal exospheric populations with the observational data on the thermal and non-thermal hydrogen fractions in the Martian corona (Clarke et al., 2024) and thereby draw important conclusions about the key processes that determine how the climate and atmosphere of Mars are changing during its evolution.

This paper presents the results of modeling the distribution of the non-thermal (hot and ENA) fractions of atomic hydrogen, carried out for known dates of HST observations (Bhattacharyya et al., 2017a; Bhattacharyya et al., 017b; Bhattacharyya et al., 2020) of the extended hydrogen corona of Mars using MAVEN measurements as input data.

2 Methods and models

2.1 Observations of the hydrogen corona of Mars by the Hubble Space Telescope

The scale height for thermal H atoms in the atmosphere is smaller for Earth and Venus due to their significant gravity compared to Mars. The resulting Martian exosphere is extended, and it is therefore difficult to observe the transition height above which the energetic non-thermal H fraction becomes dominant. To overcome this limitation, HST observations were conducted in late 2017 and early 2018 specifically targeting the non-thermal (hot) fraction of H in the uppermost hydrogen corona of Mars (Bhattacharyya et al., 2017a; Bhattacharyya et al., 2017b; Bhattacharyya et al., 2020). Because of the higher thermal H scale height values in the Martian exosphere, the HST far-UV observations were conducted during low solar activity (F10.7 < 80 on Earth) and at orbital longitudes (Ls = 108° - 128°) closest to the Martian aphelion (Ls = 71°). These observing conditions resulted in lower thermal H atom temperatures and, hence, a reduced scale height. The Earth-Mars distance was also large (1.58–1.96 au), allowing global imaging of Martian Ly-α emission at altitudes of ~33,000 km. The observations were carried out in a series of three separate sessions over a period of 2 months, namely, on 31 December 2017, 13 January 2018, and 10 February 2018. The observations with the Advanced Camera for Surveys (ACS) instrument on HST revealed the H Ly-α line emission in the extended hydrogen corona of Mars. The resulting brightness measurements of this line are shown in the left panel of Figure 1. The data reduction procedure for extracting the H Ly-α line emission from the ACS broadband far-ultraviolet images of Mars is described in the paper (Bhattacharyya et al., 2023). The radial intensity profiles in kiloRelays (1 kiloRelay = 10^9 photons/cm^2/s) for each observation day show a sharp change in slope between 5,000 and 10,000 km, as shown in the right panel of Figure 1. At these altitudes, the mean uniform atmospheric altitude scale begins to transition from a predominance of thermal H atoms to a predominance of suprathermal H atoms and is similar to the double-sloping profiles observed in the upper atmosphere of Venus (Anderson, 1976).

2.2 Fraction of suprathermal hydrogen atoms in the corona of Mars

The solar influence on the upper atmospheres of the terrestrial planets is carried out both by absorption of soft X-rays and extreme ultraviolet (EUV) solar radiation, and by the influence of solar wind plasma, and leads to the formation of an extended neutral corona populated by suprathermal (hot) atoms of H, C, N and O (in the case of Mars, see, for example, Groeller et al., 2014; Shematovich and Marov, 2018). One of the important results of the results of the MAVEN space mission was the confirmation through Imaging Ultraviolet Spectrograph (IUVS) observations of the presence of an extended corona of hydrogen, carbon, and oxygen atoms around the planet (Deighan et al., 2015). The hot corona, in turn, is modified by the influx of solar wind (SW) plasma and local fluxes of ions captured from the ionosphere into the planetary exosphere. This influx causes the formation of a flux of superthermal atoms (energetic neutral atoms - ENA) due to charge exchange of the neutral exospheric atoms with precipitating high-energy SW protons. This flux of energetic neutral atoms both penetrates into the upper atmosphere of Mars and escapes from it.

Kinetic Monte Carlo models for studying the distribution of suprathermal hydrogen atoms in the coronae of Venus, Earth, and Mars are discussed in detail in reviews (Johnson et al., 2008; Shematovich and Marov, 2018). These models consider elastic, inelastic, and superelastic (quenching of metastable excitation levels) collisions of suprathermal hydrogen atoms with atmospheric gas, and also use differential scattering cross sections that determine the scattering angles in these processes. The most important components of the developed numerical model are photochemical and plasma sources of suprathermal atoms, such as the dissociation of water molecules by solar UV radiation and the accompanying

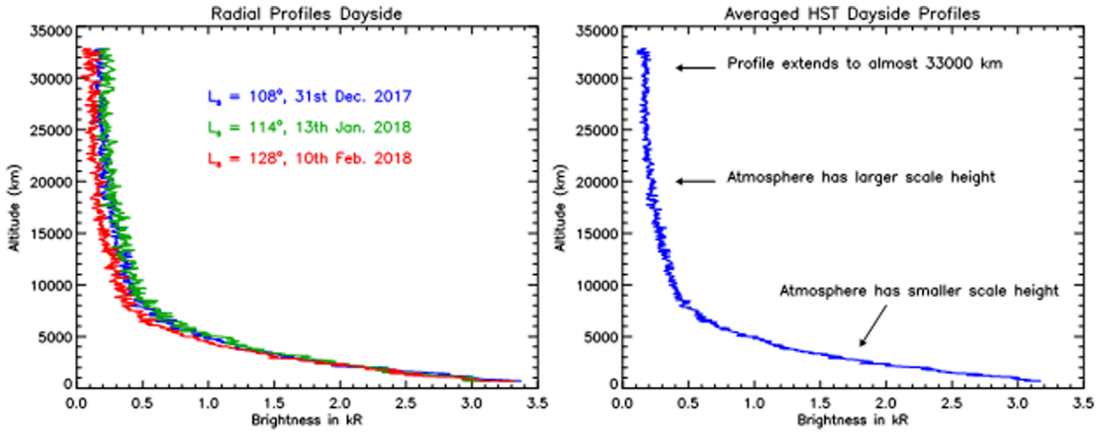

FIGURE 1
Left: Measured radial profiles of the Ly-α line brightness, constructed for three HST observation sessions in the altitude range 1–11.32R_{Mars}. *Right:* Averaged HST dayside profile of the Ly-α line brightness showing the different scale heights for H exospheric distribution. This figure has been adapted from Bhattacharyya et al. (2023).

flux of photoelectrons, dissociative recombination of molecular ions, exothermic ion-molecular reactions, and charge exchange of hydrogen atoms with solar wind protons at exospheric altitudes. The instruments onboard the MAVEN spacecraft do not allow direct measurements of the fluxes of escaping neutral H atoms, so to obtain estimates of the atmospheric loss, it is necessary to use numerical models (Chaffin et al., 2018; Jakosky et al., 2018; Ramstad et al., 2022; Bhattacharyya et al., 2023; Gregory et al., 2023) to interpret observations of planetary coronae.

Precipitating high-energy solar wind protons (H^+) and hydrogen energetic atoms (HENA) lose their kinetic energy in (a) elastic and inelastic collisions, (b) ionization of target atmospheric molecules/atoms, and (c) charge transfer and electron capture collisions with the major atmospheric constituents

$$H^+(HENA)+M\rightarrow\begin{cases}H_f^+\left(HENA_f\right)+M^* & (a)\\ H_f^+\left(HENA_f\right)+M^++e & (b)\\ HENA_f\left(H_f^+\right)+M^+(M)+(e) & (c)\end{cases}\qquad(1)$$

Here, M denotes the main atmospheric constituents - CO_2, N_2, O, and H - included in the model. Secondary hydrogen energetic atoms $HENA_f$ and protons H^+_f carry enough kinetic energy to cycle through the collisional channels in Equation 1 and result in a an ever-increasing fraction of suprathermal atoms and molecules of atmospheric gas in electronically excited states, M^*.

To study the precipitation of high-energy HENA/H^+ flux into the planetary atmosphere, we solve the kinetic Boltzmann equations (Shematovich et al., 2011; 2019; 2021) for H^+ and HENA, including the collision term:

$$\vec{v}\frac{\partial}{\partial\vec{r}}f_{HENA,H+}+\left(\vec{g}+\frac{e}{m_{H+}}\vec{v}\times\vec{B}\right)\frac{\partial}{\partial\vec{v}}f_{HENA,H+}=Q_{HENA_f,H_f^+}(\vec{v})+\sum_M J_{mt}\left(f_{HENA,H+},f_M\right)\qquad(2)$$

The Equation 2 is written in the standard form for the velocity distribution functions $f_{HENA,H+}$ (r,v) for hydrogen energetic atoms and protons, and f_M(r,v) for atmospheric species (Gérard et al., 2000). The source term Q_{HENA_f,H_f^+} describes the production rate of secondary $HENA_f/H_f^+$ particles and the elastic, and inelastic collisional terms J_{mt} for HENA/H^+ describe the energy and momentum transfer to the ambient atmospheric gas characterized by local Maxwellian velocity distribution functions. The kinetic Monte Carlo model (Gérard et al., 2000; Shematovich et al., 2011; 2021) is used to solve the kinetic Equation 2. The kinetic Monte Carlo model, which is 1D in geometric space and 3D in velocity space, is used to solve the kinetic (Equation 2). Ultimately, the 3D trajectories of the HENA/H^+ populations are calculated in the code and projected in the radial direction. The details of the model implementation and statistics control with the variance below 10% can be found in (Shematovich et al., 2019). It should be pointed out that a key aspect of this model is the probabilistic treatment of the scattering angle distribution, which influences both the energy degradation rate and the angular redistribution of the precipitating protons and hydrogen atoms (Bisikalo et al., 2018; Shematovich et al., 2019). To do this, it is necessary to use both total and differential cross sections when calculating the post-collision velocities for high-energy precipitating H/H^+ and atmospheric particles.

One of the important consequences of the penetration of a high-energy flux of protons and hydrogen atoms into the upper atmosphere is the formation of suprathermal hydrogen atoms H_h due to the transfer of momentum in elastic and inelastic collisions of the H^+ and HENA fluxes with atmospheric thermal H atoms. However, in addition to the kinetic model, it is necessary to use the results of magnetohydrodynamic (MHD) and aeronomic modeling to correctly solve the problem of non-thermal hydrogen fraction in the Martian corona. The MHD model developed by Zhilkin et al. (2022) provides a framework for simulating the interaction between stellar winds and the upper atmospheres of terrestrial planets. The results of this modeling - the energy fluxes of energetic charged particles H+/e−entering the neutral corona and the calculated positions of bow shock (BS) and induced magnetosphere boundary (IMB) - are used as initial and boundary conditions for subsequent kinetic modeling.

In our previous studies (Shematovich, 2017; Bisikalo et al., 2018; Shematovich et al., 2019), an additional source of hydrogen atom escape from the upper atmosphere of Mars due to precipitation of high-energy protons and hydrogen energetic atoms from the solar wind was investigated. Such a mechanism of atmospheric loss of the neutral upper atmosphere was first proposed in the studies of proton aurora in the upper atmosphere of the Earth (see, e.g., Bisikalo et al., 2003; Shematovich, 2013). Although proton auroral phenomena are sporadic, they are nevertheless a manifestation of increased solar activity and are accompanied by high loss rates of atomic hydrogen from the Earth's atmosphere (see, for example, Qin and Waldrop, 2016; Baliukin et al., 2019; Deighan et al. (2018)). Recent observations of proton aurorae at Mars—detected through excess Ly-α emission from atomic hydrogen (Deighan et al. (2018)) - have revealed a previously overlooked mechanism for atmospheric escape. In this study, we quantify the contribution of solar-wind-driven hydrogen precipitation (energetic H atoms) to the non-thermal hydrogen population in Mars' corona and its subsequent impact on atmospheric loss rates. This process has not been accounted for in prior analyses of Martian atmospheric escape based on MAVEN data (Jakosky et al., 2018), despite its potential significance for understanding the planet's long-term evolution.

In the numerical implementation of the kinetic Monte Carlo model of the formation, kinetics, and transport of precipitating proton and ENA fluxes from the solar wind plasma, statistics are accumulated on collisions accompanied by the formation of, for example, suprathermal hydrogen atoms H_h:

$$H^+/HENA(E) + H_{th} \rightarrow H^+/HENA(E' < E) + H_h(E'' = E - E'), \quad (3)$$

where E and E′ are the kinetic energies of the H^+/HENA particles before and after the collision, and H_{th} are the thermal hydrogen atoms from the Martian corona. The source function of suprathermal H_h atoms is determined based on statistics on all collisions in Equation 3 that occur in the studied region of the atmosphere and specifies the formation rate of suprathermal hydrogen atoms during the precipitation of energetic H^+/HENA particles. This function is further used as input data for the kinetic Monte Carlo model (Shematovich, 2017) of collisions and transport of hot hydrogen atoms in the transition region between relatively dense thermosphere and outer exosphere. Accordingly, the output data of the kinetic model (Shematovich, 2017; Shematovich et al., 2019) are the volume rates of formation of suprathermal atoms in collisions and their distribution function by kinetic energy in the studied transition region of the Martian atmosphere. This numerical model corresponds to the microscopic level of description of the gas state in the planetary corona (Shematovich and Marov, 2018); the local mean time and mean free path of hot particles at the lower boundary of the transition region, where the surrounding atmospheric gas is denser, are taken as characteristic scales of time and space. We were primarily interested in calculating the population of the extended corona of Mars by suprathermal hydrogen atoms, so the lower limit of the energy of suprathermal atoms in the model was set at 0.02 eV, which corresponds to an exospheric temperature of ~170–240 K at a low level of solar activity.

The extended hydrogen corona of Mars, which spans altitudes of 80 to 32,000 km, is studied. The lower boundary is taken to be the relatively dense thermosphere, where hot particles quickly lose excess kinetic energy in collisions with thermal molecules of carbon dioxide and oxygen. The upper boundary is taken much higher than the exobase (~190 km), where gas flow becomes freely molecular, and because the extended hydrogen corona was observed by HST in the height range $(1–11.32)R_{Mars}$. The studied region is divided into cells with a step of 5 km. In each cell, the atmospheric gas, consisting of CO_2 and N_2 molecules and O and H atoms, is represented by model particles with specified concentrations and temperatures according to the model calculations (Bougher et al., 2017). In each cell, model particles H_h are born that correspond in the physical model to the source function of suprathermal hydrogen atoms in Equation 3, which move in the gravitational field of Mars and collide with atmospheric gas, producing secondary suprathermal particles. Since the modeling is carried out at the molecular level, detailed statistics are accumulated on the spatial distribution of suprathermal hydrogen atoms by velocity (kinetic energy) and on the energy spectra of particle fluxes, both populating the hot hydrogen corona and escaping from the atmosphere of Mars.

Here, we outline the background of the kinetic Monte Carlo (KMC) models employed in this study. Proton auroral events observed on the dayside of Mars (Hughes et al., 2019) are driven by fluxes of energetic hydrogen atoms penetrating the atmosphere (Deighan et al., 2018; Henderson et al., 2021). To quantify this process, we used a KMC model (Shematovich et al., 2019) to calculate the source function of suprathermal hydrogen atoms. This involved simulating the charge exchange of solar wind protons in Mars' extended hydrogen corona using a kinetic model (Shematovich et al., 2019; Shematovich et al., 2021), which yielded the energy spectra of HENAs entering the atmosphere across the induced magnetosphere boundary. The IMB position was derived from an MHD model (Zhilkin et al., 2022). These HENA spectra served as the upper boundary condition for a KMC model (Shematovich et al., 2019), simulating HENA precipitation into the upper atmosphere. This enabled numerical estimation of the production rates and energy spectra of suprathermal hydrogen atoms generated via elastic and inelastic collisions between HENAs and exospheric thermal hydrogen atoms. Finally, the derived suprathermal hydrogen formation rates were used as input for a second KMC model (Shematovich, 2017) to study the kinetics and transport of these hot atoms in Mars' hydrogen corona (see Figure 2 for a schematic of the coupled models).

To estimate the contribution of an additional source of suprathermal hydrogen atoms during proton auroral events on the formation of the hot extended hydrogen corona, the following inputs were used:

- A model neutral atmosphere, in which the temperature and density profiles of the main components of CO_2, CO, and O in the upper atmosphere were taken from the model (Bougher et al., 2017) for the date 13 January 2018, when observation of the hydrogen luminosity in the Ly-α line in the extended corona of Mars were made (Bhattacharyya et al., 2020). The distribution of hydrogen atoms in the extended corona of Mars was provided by the MAVEN team (dashed blue line shown in Bhattacharyya et al. (2023)) for the same date. This height profile of the thermal H is also shown by solid blue line in the panel (A) of Figure 9.

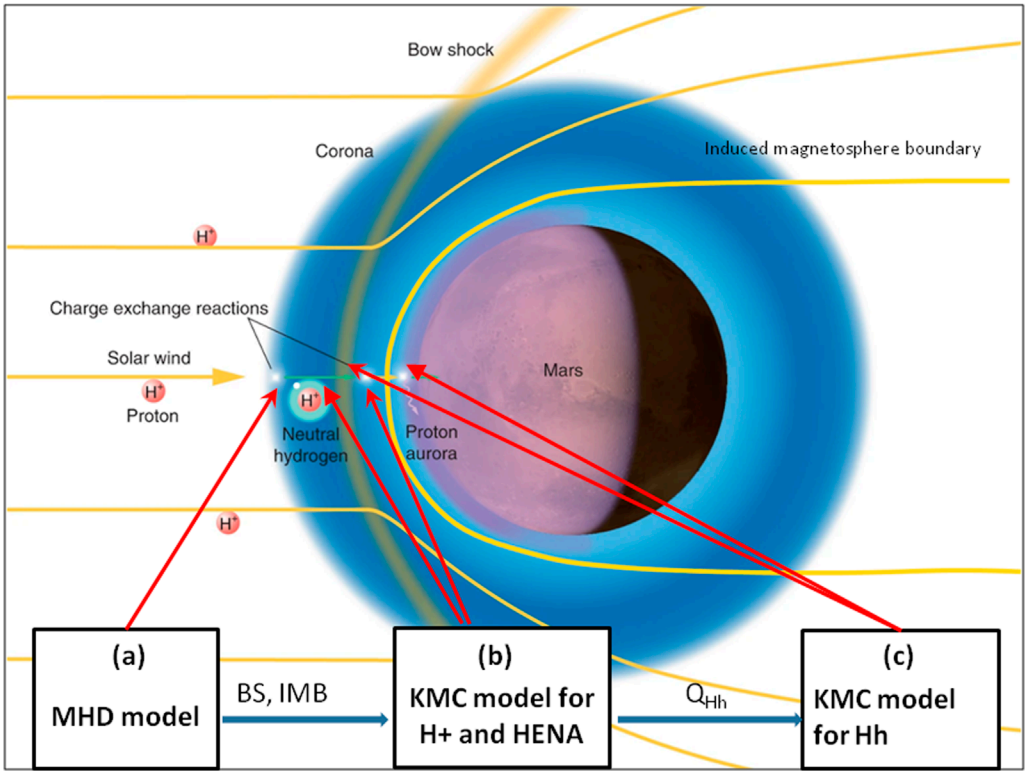

FIGURE 2
The extended hydrogen corona at Mars under the solar forcing (adapted from Deighan et al., 2018). The numerical framework used to quantify non-thermal hydrogen populations in Mars' corona consists of three coupled models: **(a)** global MHD model (Zhilkin et al., 2022) which simulates solar wind forcing on the neutral atmosphere and determines the positions of plasma boundaries, specifically the bow shock and induced magnetosphere boundary; **(b)** the kinetic Monte Carlo (KMC) model (Shematovich et al., 2019; Shematovich et al., 2021) which uses MHD-derived boundaries to compute energy spectra of hydrogen energetic neutral atoms generated through solar wind proton charge exchange and derives the source function Q_{Hh} for suprathermal hydrogen produced via collisional processes (see Equation 3); **(c)** kinetic Monte Carlo model (Shematovich, 2017) which propagates the source function Q_{Hh} through the exosphere to resolve the kinetics and spatial distribution of the hot hydrogen population and provides altitude-dependent densities and escape fluxes of suprathermal hydrogen in the Martian corona.

- The energy flux and energy spectrum of protons from the undisturbed solar wind measured by the MAVEN Solar Wind Ion Analyzer (SWIA) (Halekas et al., 2015) for the above-mentioned observation date was provided by the SWIA team (solid green line shown in paper by Bhattacharyya et al. (2023)). This omnidirectionally averaged spectrum of solar wind protons was used as a boundary condition at an altitude of 32,000 km for the kinetic Monte Carlo model (Shematovich et al., 2021) and is shown by green line in panels (a) in Figures 4, 5.

The spectra of HENAs obtained in these calculations are taken as the upper boundary condition for the kinetic Monte Carlo model (Shematovich et al., 2019) of the precipitation of hydrogen atoms with high energies into the upper atmosphere through the boundary of the induced magnetosphere at an altitude of 820 km, which made it possible to calculate the altitude profiles of the volumetric formation rate and the energy spectra of hydrogen atoms formed in collisions shown by Equation 3 with suprathermal energies (Shematovich and Bisikalo, 2020; 2021; Zhilkin et al., 2022).

3 Results

The model runs were performed for a solar zenith angle of 0°. The calculation results are shown in Figures 3–9. From the calculations performed using the kinetic Monte Carlo model (Shematovich et al., 2019), it is evident that the production of suprathermal H atoms occurs predominantly in the transition region near and above the exobase, where the statistics of HENA collisions with thermal exospheric hydrogen atoms is quite high. In numerical implementations of the kinetic Monte Carlo model of the hot hydrogen corona (Shematovich, 2017), statistics of the distributions of supra- and super-thermal hydrogen atoms by kinetic energies in all computational cells were accumulated. Both energy distribution functions and energy spectra of downward and upward fluxes of hydrogen atoms with an excess of kinetic energy characterize the non-thermal fractions of H atoms populating the extended corona at Mars. Figure 3 shows the calculated energy distribution functions (EDFs) of supra- (bottom panel) and super- (top panel) thermal hydrogen atoms at altitudes of 200 km, 500 km, and 1,500 km in the extended corona of Mars for the date of 13 January 2018. Calculations of EDFs are given for an altitude of

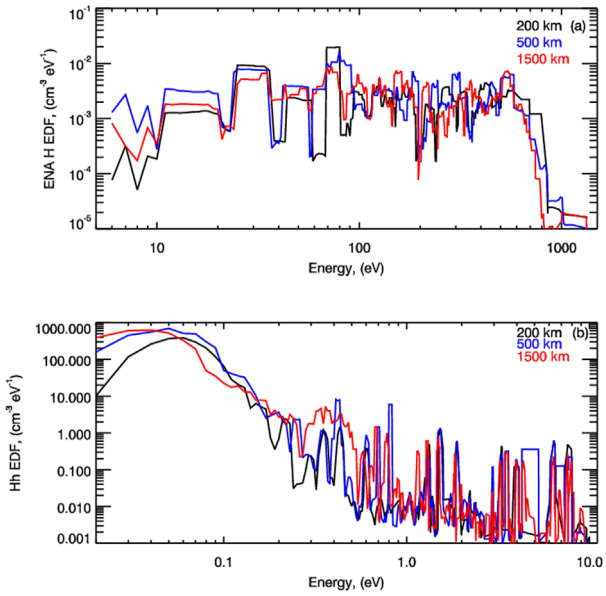

FIGURE 3
Energy distribution functions of superthermal HENA **(a)** and suprathermal H_h **(b)** hydrogen atoms at different altitudes in the extended hydrogen corona. The calculations were performed using the kinetic Monte Carlo model (Shematovich, 2017) for date of the HST observations obtained on 13 January 2018. The simulations were conducted using the base kinetic model, with the induced magnetosphere boundary set at an altitude of 820 km.

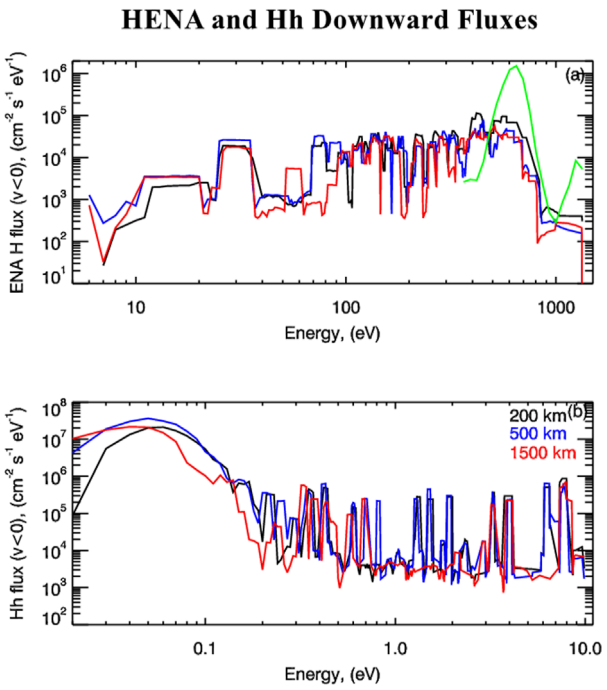

FIGURE 4
Energy spectra of the downward fluxes of superthermal HENA **(a)** and suprathermal H_h **(b)** hydrogen atoms at different heights in the extended hydrogen corona. The average spectrum of precipitating solar wind protons measured by MAVEN SWIA is shown by the green line in panel **(a)**. The calculation was performed using the kinetic Monte Carlo model (Shematovich, 2017; Shematovich et al., 2021) for date of the HST observations performed on 13 January 2018. The simulations were conducted using the base kinetic model, with the induced magnetosphere boundary set at an altitude of 820 km.

200 km, corresponding to the production peak of suprathermal hydrogen atoms during the precipitation of HENA formed in the process of the charge exchange of high-energy hydrogen atoms with solar wind protons. The calculations reveal that the energy distribution functions of suprathermal hydrogen atoms exhibit a markedly non-equilibrium character, as evidenced by extended tails in the EDFs reaching up to several eV. These features arise from the collision processes described by Equation 3.

The energy spectra of the downward and upward fluxes of superthermal HENA (A) and suprathermal H_h (B) hydrogen atoms at different altitudes in the extended hydrogen corona are given in Figures 4, 5, respectively. The spectrum of precipitating solar wind protons measured by MAVEN SWIA is shown by the green line in panels (A) of both figures. The simulations were conducted using the base kinetic model, with the induced magnetosphere boundary set at an altitude of 820 km and for data inputs corresponding to the HST observations on 13 January 2018. General structure of both energy distribution functions and energy spectra of energy fluxes is characterized by the formation of Maxwellian cores at energies below 0.2 eV and extended non-Maxwellian tails for energies above 0.2 eV for suprathermal H atoms formed in the collisions summarized in Equation 3 in the transition region between thermosphere and exosphere. The stochastic nature of these distribution tails arises from the low collision statistics occurring above the exobase.

As for the distribution of suprathermal HENAs in the extended hydrogen corona shown in the top panels of Figures 4, 5, their form is determined by the collisional degradation of the initial HENA distribution formed in the region of charge exchange with the solar wind protons. It is known that the efficiency of this process does not exceed 4%–8% depending on the thermal H content in the corona (Shematovich, Bisikalo, 2021) and the energy spectrum of the initial HENA flux coincides with the energy spectrum of protons from the undisturbed solar wind (Shematovich, and Bisikalo, 2020; Shematovich et al., 2021).

By integrating the energy spectra of downward and upward energy fluxes for both supra- and super-thermal hydrogen atoms across all computational cells, we obtained the altitude profiles of non-thermal hydrogen atom fluxes in Mars' extended corona. They are shown in Figure 6, where downward fluxes are indicated by blue lines and upward fluxes - by red lines. The superthermal HENAs are shown by solid lines, while the suprathermal atoms - by dashed lines.

It is seen that efficiency of charge exchange is about 6% and is determined by the content of thermal H provided by MAVEN measurements (Bougher et al., 2017; Bhattacharyya et al., 2023). Energy transfer from ENAs penetrating through the induced magnetosphere boundary to the thermal exospheric H atoms occurs in the transition region near the exobase and results in the population of upper layers of the exosphere and formation of escaping flux of the hot H atoms.

The escape energy for atomic hydrogen from the Martian atmosphere is ~0.05 eV near the exobase. The calculated steady-state energy distribution functions in Figure 3 reveal a significant

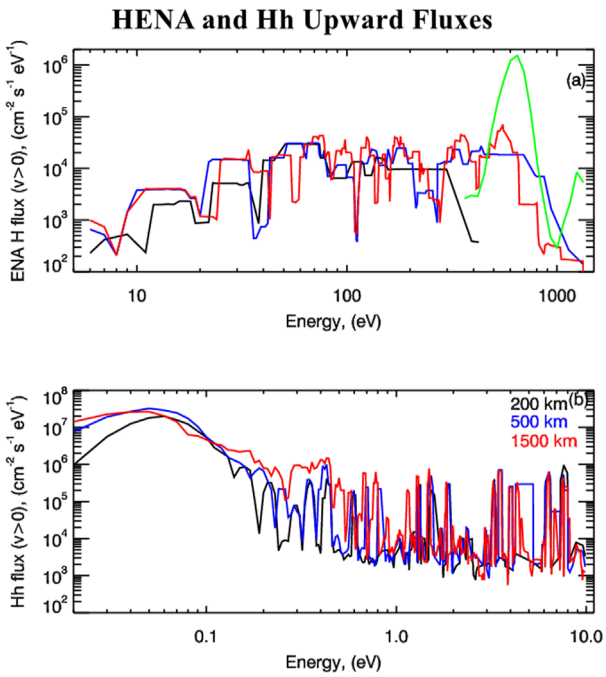

FIGURE 5
Same as Figure 4 but for upward fluxes of superthermal HENA **(a)** and suprathermal H_h **(b)** hydrogen atoms at different heights in the extended hydrogen corona.

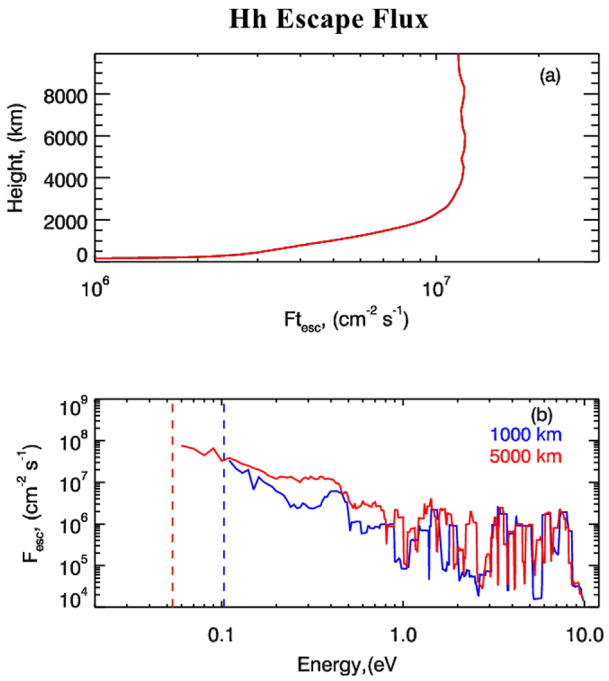

FIGURE 7
(a) Altitude profile of the escape flux of suprathermal (hot) H atoms formed due to the HENA precipitation. The calculation was done for the observation date of 13 January 2018. **(b)** Energy spectrum of the escaping flux of suprathermal H atoms at heights of 1,000 and 5,000 km. The vertical lines show the escape energies from the Martian atmosphere for indicated heights.

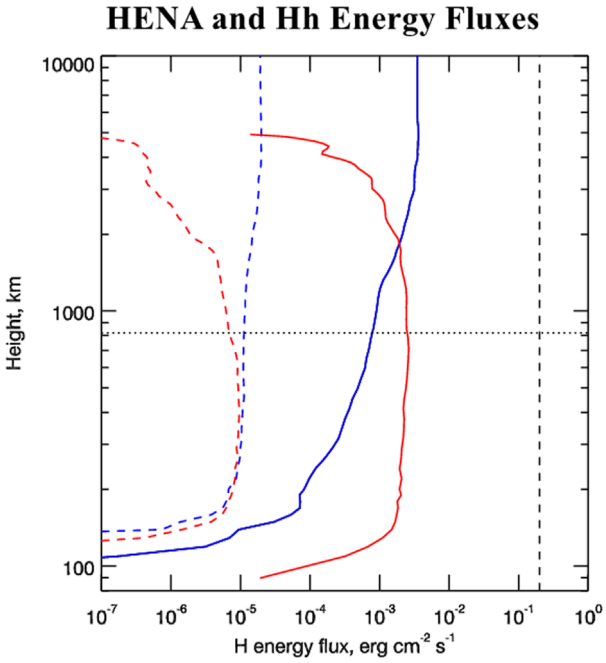

FIGURE 6
Height profiles of downward (blue lines) and upward (red lines) energy fluxes of superthermal HENA (solid lines) and suprathermal H_h (dashed lines) hydrogen atoms. The vertical, dashed line shows the energy flux of the incoming solar wind at the model upper boundary. The horizontal dotted line shows the height of induced magnetosphere boundary.

population in the suprathermal energy range (up to 0.05 eV). This population arises from elastic collisions between hydrogen energetic neutral atoms and thermal hydrogen atoms, which contribute an additional suprathermal hydrogen component to Mars' hot corona. Calculations have shown that the EDFs of hydrogen atoms are of a substantially nonequilibrium nature compared to the thermal fraction of the hydrogen corona, since there is a significant fraction of hydrogen atoms in the suprathermal energy region (0.02–10 eV) at altitudes above the exobase (i.e., 180–200 km), and the hot corona is predominantly populated by suprathermal H atoms due to their transfer from the underlying layers of the thermosphere. This leads to the fact that the number of particles with energies exceeding the escape energy becomes greater in the corona than at altitudes below the exobase, where suprathermal particles effectively lose excess kinetic energy in frequent collisions with atomic oxygen and carbon dioxide molecules. Moreover, as it is seen from Figures 3–5, the HENA precipitation leads to the formation of extended tails in the distribution of hydrogen atoms in the region of superthermal (E > 0.02 eV) energies.

Figure 7 shows the altitude profile of the suprathermal hydrogen atom escape flux (upper panel) formed due to the precipitation of ENA H after the charge exchange of solar wind protons in the extended hydrogen corona of Mars. The lower panel of Figure 5a shows the energy spectra of the upward flux of suprathermal H atoms calculated at altitudes of 1,000 km and 5,000 km. The calculations refer to the date of 13 January 2018. The calculations show that integrating the energy spectrum above the local escape

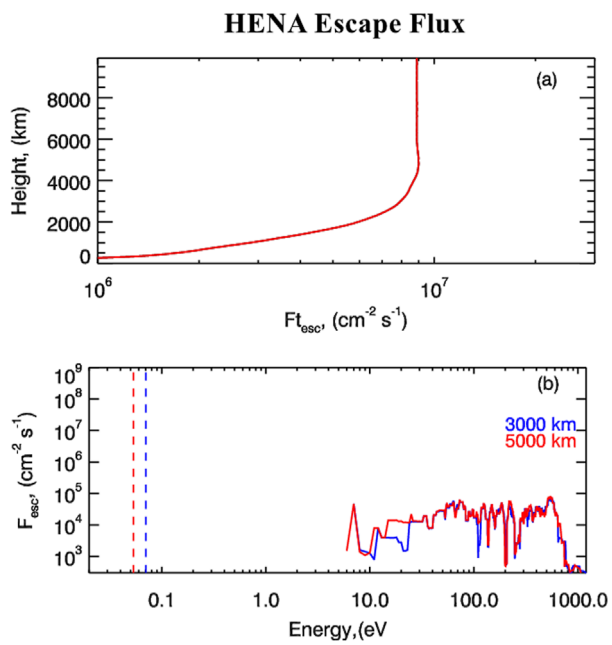

FIGURE 8
(a) Altitude profile of the escape flux of superthermal HENA atoms formed due to the forcing by solar wind. The calculation was done for the observation date of 13 January 2018. **(b)** Energy spectrum of the escaping flux of superthermal H atoms at heights of 3,000 and 5,000 km. The vertical lines show the escape energies from the Martian atmosphere for indicated heights.

energy yields an estimated escape flux of suprathermal hydrogen atoms of ~1.1×10^7 cm^{-2} s^{-1}. The obtained estimate corresponds to ~26–30% of the rate of thermal escape of H from the corona of Mars (Chaffin et al., 2018; Chaufray et al., 2024; Yelle, 2024). It should be noted that the calculations presented here were carried out for conditions of low solar activity and at Mars's aphelion. We find that even for such conditions of solar activity in aeronomic models of water loss from the Martian atmosphere (Jakosky, 2024; Clarke et al., 2024), it is necessary to take into account non-thermal mechanisms of hydrogen loss. The active Sun increases the modern rate of hydrogen loss and, accordingly, the early Sun with high radiation fluxes in soft X-rays and extreme ultraviolet probably contributed to a significant loss of water from the atmosphere of Mars on astronomical time scales (Jakosky, 2021; 2024; Clarke et al., 2024).

The similar estimate of escaping flux of superthermal HENAs is shown in Figure 8. The resulting escape flux of superthermal H atoms reaches the value of ~$9.\times10^6$ cm^{-2} s^{-1}, and its energy spectrum corresponds to the fraction of the ENA H flux backscattered by the Martian atmosphere (Shematovich et al., 2021).

The kinetic Monte Carlo model allows us to calculate the EDF of supra- and superthermal H atoms from the kinetic energy in each radial cell. Height profiles of bulk characteristics of non-thermal hydrogen populations based upon these EDFs are estimated and are shown in Figure 9. Height profiles of the number densities (*top panel)* with the black line showing the total density of hydrogen atoms, mean kinetic energies (*middle panel)*, and bulk velocities of the thermal (*blue lines*), suprathermal (*red lines*) and superthermal (*magenta lines*) fractions of atomic hydrogen in the extended corona of Mars are presented in this figure. The calculations were conducted for date of 13 January 2018, when the HST observations of the luminosity in the hydrogen Ly-α line of the Mars corona had been done. The black lines show the total density and mean kinetic energy of hydrogen atoms. In fact, these characteristics of the supra- and super-thermal fractions of atomic hydrogen allowed us to estimate the population of the extended hot hydrogen corona of Mars during proton auroral events (Hughes et al., 2023). The altitude profiles of non-thermal hydrogen fractions exhibit a distinct slope transition between 5,000 and 10,000 km, marking the atmospheric region where the dominant population shifts from thermal to non-thermal hydrogen, consistent with HST observations (Bhattacharyya et al., 2023).

Although proton auroras are sporadic events, the source of hot hydrogen atoms induced by precipitation processes can become dominant for the population of the hydrogen corona under conditions of extreme solar events - solar flares and coronal mass ejections - as shown by recent observations of the MAVEN spacecraft (Halekas, 2017; Jakosky et al., 2018; Henderson et al., 2021). The studied mechanism of the formation of the supra- and super-thermal fractions in the corona and the escape flux of hydrogen atoms due to atmospheric sputtering induced by the solar wind forcing on Mars should be taken into account, in particular, in studies of the evolution of the planet's climate on geological time scales.

4 Discussion and conclusion

In this study, we present computational results characterizing the penetration of undisturbed solar wind protons into Mars' dayside atmosphere through charge exchange processes within the extended hydrogen corona (Shematovich et al., 2021). Our approach enabled the self-consistent calculation of (1) production sources for both supra- and super-thermal hydrogen atoms and (2) their subsequent kinetics and transport dynamics.

The non-thermal fractions of H atoms are present in the exospheres of all terrestrial planets in the Solar System. Using a kinetic Monte Carlo model, we calculated the density distribution of non-thermal (supra- and super-thermal) H atoms in Mars' extended corona. The modeling approach consisted of two steps. At first step, we simulated the penetration of the undisturbed solar wind into the hydrogen corona resulting in the flux of HENAs penetrating into the neutral atmosphere through the induced magnetosphere boundary. This step yielded source functions representing both the formation rates and energy spectra of suprathermal H atoms generated by HENA precipitation in the upper atmosphere. At second step, we modeled the collisional relaxation and transport of suprathermal H atoms through the extended hydrogen corona using these source functions as input. This self-consistent approach allowed us to determine both the density distribution and escape fluxes of non-thermal H atoms in Mars' exosphere, which result from collisions between HENAs and thermal exospheric H atoms. The main limitations of both steps in the kinetic modeling are the scarcity of laboratory data on total and differential scattering cross-sections for collisions involving supra- and super-thermal hydrogen atoms with thermal H atoms in the Martian exosphere.

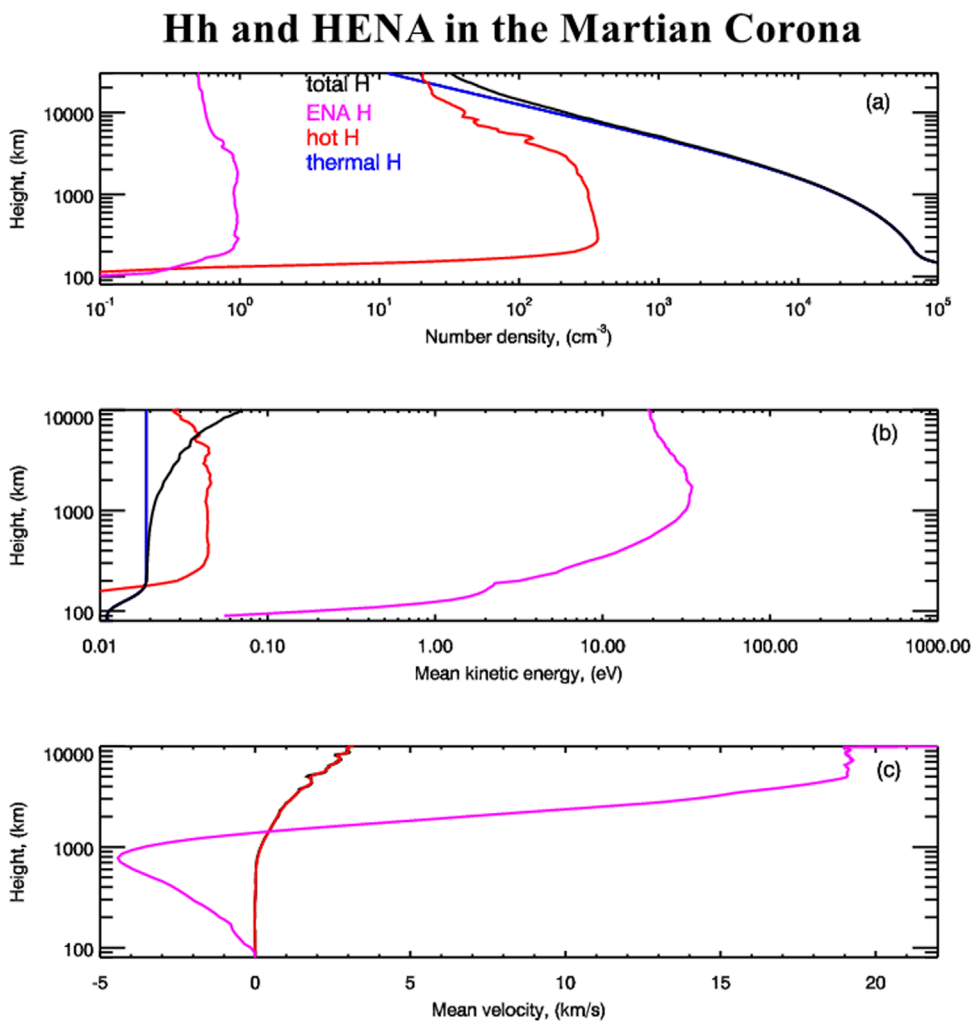

FIGURE 9
Height profiles of the thermal (blue lines), suprathermal (red lines), and superthermal (magenta lines) fractions of atomic hydrogen in the extended corona of Mars. **(a)** Number densities of atomic hydrogen populations with black line showing the total density of hydrogen atoms. **(b)** Mean kinetic energy of atomic hydrogen populations. **(c)** Bulk velocity of atomic hydrogen populations. The calculation results are given for date of 13 January 2018, when the HST observations of the luminosity in the hydrogen Ly-α line of the Mars corona had been done.

The non-thermal fractions of H atoms populating the extended Martian corona should be taken into account in the aeronomic models used for interpretation of the *in situ* and remote measurements of the planet's neutral gaseous environment. Furthermore, hydrogen escape rates through non-thermal processes were likely significantly enhanced during the early periods of Martian history, when the Sun was younger and more active. During this period, increased charge exchange between solar wind protons and coronal hydrogen atoms would have accelerated planetary water loss (Jakosky, 2021). These findings suggest that Mars may have lost most of its water during the planet's early evolutionary stages. Consequently, investigation of the formation and evolution of non-thermal hydrogen fractions in planetary coronae is crucial for reconstructing the long-term water loss history of terrestrial planets, and assessing the potential for life to have emerged and persisted on these worlds.

This study demonstrates that charge exchange between solar wind protons and thermal hydrogen atoms in Mars' extended corona serves as an active aeronomic mechanism for generating non-thermal hydrogen fractions - a process that may similarly influence other terrestrial planets. Enhanced solar activity would consequently amplify both thermal and non-thermal hydrogen escape rates while increasing the abundance of supra- and super-thermal H atoms in the corona. These findings necessitate incorporating both non-thermal hydrogen fractions when interpreting space-based observations of hot planetary coronae (Bhattacharyya et al., 2023), particularly during periods of high solar activity. Future investigations should prioritize Mars' perihelion season (Ls = 180°–330°), coinciding with - higher thermal H densities, increased solar plasma flux, and frequent dust storms - conditions that likely intensify non-thermal hydrogen population dynamics. The production of suprathermal H atoms - generated through collisions between thermal H atoms and HENAs formed via solar wind charge exchange - leads to enhanced non-thermal hydrogen escape during Martian perihelion. This process likely contributes to seasonal increases

in planetary water loss. During the early periods of Martian history, when the young Sun exhibited higher XUV flux and greater solar wind activity, charge exchange with exospheric hydrogen would have been more frequent and intense (Bhattacharyya et al., 2023; Clarke et al., 2024; Jakosky, 2024). These conditions would have driven substantially greater non-thermal escape, potentially accounting for a significant fraction of Mars' long-term water loss.

Data availability statement

The original contributions presented in the study are included in the article/supplementary material, further inquiries can be directed to the corresponding author.

Author contributions

VS: Conceptualization, Data curation, Investigation, Methodology, Supervision, Visualization, Writing – original draft, Writing – review and editing. DB: Conceptualization, Methodology, Software, Writing – review and editing.

Funding

The author(s) declare that financial support was received for the research and/or publication of this article. This work was supported by the Russian Science Foundation under Grant 22-12-00364-П.

Acknowledgments

The authors thank Drs. D. Bhattacharyya and J. T. Clarke for important discussions on HST observations of the extended hydrogen corona at Mars, and A. Zhilkin for significant help with the MHD modeling.

Conflict of interest

The authors declare that the research was conducted in the absence of any commercial or financial relationships that could be construed as a potential conflict of interest.

Generative AI statement

The author(s) declare that no Generative AI was used in the creation of this manuscript.

Publisher's note

References

Anderson, D. E., Jr., and Hord, C. W. (1971). Mariner 6 and 7 ultraviolet spectrometer experiment: analysis of hydrogen lyman-alpha data. *J. Geophys. Res.* 76, 6666–6673. doi:10.1029/JA076i028p06666

Anderson, Jr., D. E. (1974). Mariner 6, 7, and 9 ultraviolet spectrometer experiment: analysis of hydrogen lyman alpha data. *J. Geophys. Res.* 79, 1513–1518. doi:10.1029/JA079i010p01513

Anderson, Jr., D. E. (1976). The mariner 5 ultraviolet photometer experiment – analysis of hydrogen lyman alpha data. *J. Geophys. Res.* 81, 1213–1216. doi:10.1029/ja081i007p01213

Baliukin, I., Bertaux, J.-L., Quemerais, E., Izmodenov, V., and Schmidt, W. (2019). SWAN/SOHO Lyman-α mapping: the hydrogen geocorona extends well beyond the Moon. *J. Geophys. Res. Space Phys.* 124, 861–885. doi:10.1029/2018JA026136

Barth, C. A., Fastie, W. G., Hord, C. W., Pearce, J. B., Kelly, K. K., Anderson, G. P., et al. (1970). Mariner 6 and 7 ultraviolet spectrometer experiment: upper atmosphere data. *J. Geophys. Res.* 76, 2213–2227. doi:10.1029/ja076i010p02213

Barth, C. A., Fastie, W. G., Hord, C. W., Pearce, J. B., Kelly, K. K., Stewart, A. I., et al. (1969). Mariner 6: ultraviolet spectrum of Mars upper atmosphere. *Science* 165, 1004–1005. doi:10.1126/science.165.3897.1004

Bergsten, G. J., Pascucci, I., Mulders, G. D., Fernandes, R. B., and Koskinen, T. T. (2024). The demographics of Kepler's earths and super-earths into the habitable zone. *Astron. J.* 164 (21pp), 190. doi:10.3847/1538-3881/ac8fea

Bhattacharyya, D., Chaufray, J.-Y., Mayyasi, M., Clarke, J. T., Stone, S., Yelle, R., et al. (2020). Two-dimensional model for the martian exosphere: applications to hydrogen and deuterium Lyman alpha observations. *Icarus* 339, 113573. doi:10.1016/j.icarus.2019.113573

Bhattacharyya, D., Clarke, J. T., Bertaux, J.-L., Chaufray, J.-Y., and Mayyasi, M. (2015). A strong seasonal dependence in the martian hydrogen exosphere. *Geophys. Res. Lett.* 42, 8678–8685. doi:10.1002/2015gl065804

Bhattacharyya, D., Clarke, J. T., Bertaux, J.-L., Chaufray, J.-Y., and Mayyasi, M. (2017b). Analysis and modeling of remote observations of the martian hydrogen exosphere. *Icarus* 281, 264–280. doi:10.1016/j.icarus.2016.08.034

Bhattacharyya, D., Clarke, J. T., Chaufray, J.-Y., Mayyasi, M., Bertaux, J.-L., Chaffin, M. S., et al. (2017a). Seasonal changes in hydrogen escape from Mars through analysis of HST observations of the martian exosphere near perihelion. *J. Geophys. Res.* 122, 11756–11764. doi:10.1002/2017ja024572

Bhattacharyya, D., Clarke, J. T., Mayyasi, M., Shematovich, V., Bisikalo, D., Chaufray, J.-Y., et al. (2023). Evidence of non-thermal hydrogen in the exosphere of Mars resulting in enhanced water loss. *J. Geophys. Res. Planets* 128, e2023JE007801. doi:10.1029/2023je007801

Bisikalo, D. V., Shematovich, V. I., Gerard, J.-C., and Hubert, B. (2018). Monte Carlo Simulations of the interaction of fast proton and hydrogen atoms with the martian atmosphere and comparison with *in situ* measurements. *J. Geophys. Res. Space Phys.* 123, 5850–5861. doi:10.1029/2018ja025400

Bisikalo, D. V., Shematovich, V. I., Kaygorodov, P. V., and Zhilkin, A. G. (2021). Gas envelopes of exoplanets — hot Jupiters. *Phys. Uspekhi* 64, 747–800. doi:10.3367/UFNe.2020.11.038879

Bougher, S., Roeten, K. J., Olsen, K., Mahaffy, P. R., Benna, M., Elrod, M., et al. (2017). The structure and variability of Mars dayside thermosphere from MAVEN NGIMS and IUVS measurements: seasonal and solar activity trends in scale heights and temperatures. *J. Geophys. Res. Space Phys.* 122, 1296–1313. doi:10.1002/2016JA023454

Brain, D. A., Bagenal, F., Ma, Y.-J., Nilsson, H., and Stenberg Wieser, G. (2017). Atmospheric escape from unmagnetized bodies. *J. Geophys. Res. Planets* 121, 2364–2385. doi:10.1002/2016JE005162

Carr, M. H., and Head, J. W. (2003). Oceans on Mars: an assessment of the observational evidence and possible fate. *J. Geophys. Res. Planets* 108, 5042. doi:10.1029/2002JE001963

Carruthers, G. R., Page, T., and Meier, R. R. (1976). Apollo 16 Lyman alpha imagery of the hydrogen geocorona. *J. Geophys. Res.* 81, 1664–1672. doi:10.1029/JA081i010p01664

Chaffin, M. S., Chaufray, J.-Y., Deighan, J., Schneider, N. M., Mayyasi, M., Clarke, J. T., et al. (2018). Mars H escape rates derived from MAVEN/IUVS Lyman alpha brightness measurements and their dependence on model assumptions. *J. Geophys. Res. Planets* 123, 2192–2210. doi:10.1029/2018je005574

Chaffin, M. S., Chaufray, J.-Y., Stewart, I., Montmessin, F., Schneider, N. M., and Bertaux, J. L. (2014). Unexpected variability of martian hydrogen escape. *Geophys. Res. Lett.* 41, 314–320. doi:10.1002/2013GL058578

Chaffin, M. S., Kass, D. M., Aoki, S., Fedorova, A. A., Deighan, J., Connour, K., et al. (2021). Martian water loss to space enhanced by regional dust storms. *Nat. Astr.* 5, 1036–1042. doi:10.1038/s41550-021-01425-w

Chamberlain, J. W. (1963). Planetary coronae and atmospheric evaporation. *Planet. Space Sci.* 11, 901–960. doi:10.1016/0032-0633(63)90122-3

Chaufray, J.-Y., Bertaux, J.-L., LeBlanc, F., and Quemerais, E. (2008). Observation of the hydrogen corona with SPICAM on Mars express. *Icarus* 195, 598–613. doi:10.1016/j.icarus.2008.01.009

Chaufray, J.-Y., Bertaux, J.-L., Quemerais, E., Villard, E., and Leblanc, F. (2012). Hydrogen density in the dayside Venusian exosphere derived from Lyman-alpha observations by SPICAV on Venus Express. *Icarus* 217, 767–778. doi:10.1016/j.icarus.2011.09.027

Chaufray, J.-Y., Gonzalez-Galindo, F., Leblanc, F., Modolo, R., Vals, M., Montmessin, F., et al. (2024). Simulations of the hydrogen and deuterium thermal and non-thermal escape at Mars at Spring Equinox. *Icarus* 418, 116152. doi:10.1016/j.icarus.2024.116152

Chaufray, J.-Y., Modolo, R., Leblanc, F., Chanteur, G., Johnson, R. E., and Luhmann, J. G. (2007). Mars solar wind interaction: formation of the Martian corona and atmospheric loss to space. *J. Geophys. Res.* 112, E09009. doi:10.1029/2007JE002915

Clarke, J. T., Bertaux, J.-L., Chaufray, J.-Y., Gladstone, G., Quemerais, E., Wilson, J., et al. (2014). A rapid decrease of the hydrogen corona of Mars. *Geophys. Res. Lett.* 41, 8013–8020. doi:10.1002/2014GL061803

Clarke, J. T., Mayyasi, M., Bhattacharyya, D., Chaufray, J.-Y., Schneider, N., Jakosky, B., et al. (2024). Martian atmospheric hydrogen and deuterium: seasonal changes and paradigm for escape to space. *Sci. Adv.* 10, eadm7499. doi:10.1126/sciadv.adm7499

Clarke, J. T., Mayyasi, M., Bhattacharyya, D., Schneider, N. M., McClintock, W. E., Deighan, J. I., et al. (2017). Variability of D and H in the martian upper atmosphere observed with the MAVEN IUVS echelle channel. *J. Geophys. Res. Space Phys.* 122, 2336–2344. doi:10.1002/2016JA023479

Cockell, C. S., Bush, T., Bryce, C., Direito, S., Fox-Powell, M., Harrison, J. P., et al. (2016). Habitability: a review. *Astrobiology* 16, 89–117. doi:10.1089/ast.2015.1295

Deighan, J., Chaffin, M. S., Chaufray, J.-Y., Stewart, A. I. F., Schneider, N. M., Jain, S. K., et al. (2015). MAVEN IUVS observation of the hot oxygen corona at Mars. *Geophys. Res. Lett.* 42, 9009–9014. doi:10.1002/2015gl065487

Deighan, J., Jain, S. K., Chaffin, M. S., Fang, X., Halekas, J. S., Clarke, J. T., et al. (2018). Discovery of a proton aurora at Mars. *Nat. Astron.* 2, 802–807. doi:10.1038/s41550-018-0538-5

Gerard, J.-C., Hubert, B., Bisikalo, D. V., and Shematovich, V. I. (2000). Ly-alpha emission in the proton aurora. *J. Geophys. Res.*, 105, 15795–15806. doi:10.1029/1999JA002002

Gregory, B. S., Chaffin, M. S., Elliott, R. D., Deighan, J., Groeller, H., and Cangi, E. (2023). Nonthermal hydrogen loss at Mars: contributions of photochemical mechanisms to escape and identification of key processes. *J. Geophys.Res. Planets* 128, e2023JE007802. doi:10.1029/2023je007802

Gröller, H., Lichtenegger, H. I. M., Lammer, H., and Shematovich, V. I. (2014). Hot oxygen and carbon escape from the martian atmosphere. *Planet. Space Sci.* 98, 93–105. doi:10.1016/j.pss.2014.01.007

Halekas, J., Lillis, R. J., Mitchell, D. L., Cravens, T. E., Mazelle, C., Connerney, J. E. P., et al. (2015). MAVEN observations of solar wind hydrogen deposition in the atmosphere of Mars. *Geophys. Res. Lett.* 42, 8901–8909. doi:10.1002/2015gl064693

Halekas, J. S. (2017). Seasonal variability of the hydrogen exosphere of Mars. *J. Geophys. Res. Planets* 122, 901–911. doi:10.1002/2017JE005306

Henderson, S., Halekas, J., Lillis, R., and Elrod, M. (2021). Precipitating solar wind hydrogen as observed by the MAVEN spacecraft: distribution as a function of column density, altitude, and solar zenith angle. *J. Geophys. Res. Planets* 126, e2020JE006725. doi:10.1029/2020JE006725

Hughes, A., Chaffin, M., Mierkiewicz, E., Deighan, J., Jain, S., Schneider, N., et al. (2019). Proton aurora on Mars: a dayside phenomenon pervasive in southern summer. *J. Geophys. Res. Space Phys.* 124 (10), 10533–10548. doi:10.1029/2019JA027140

Hughes, A. C. G., Chaffin, M., Mierkiewicz, E., Deighan, J., Jolitz, R. D., Kallio, E., et al. (2023). Advancing our understanding of Martian proton aurora through a coordinated multi-model comparison campaign. *J. Geophys. Res. Space Phys.* 128, e2023JA031838. doi:10.1029/2023JA031838

Hunten, D. M., and McElroy, M. B. (1970). Production and escape of hydrogen on Mars. *J. Geophys. Res.* 75, 5989–6001. doi:10.1029/ja075i031p05989

Jakosky, B. (2021). Atmospheric loss to space and the history of water on Mars. *Ann. Rev. Earth Plan. Sci.* 49, 71–93. doi:10.1146/annurev-earth-062420-052845

Jakosky, B. M. (2024). The present epoch may not be representative in determining the history of water on Mars. *PNAS* 121 (52), e2321080121. doi:10.1073/pnas.2321080121

Jakosky, B. M., Brain, D., Chaffin, M., Curry, S., Deighan, J., Grebowsky, J., et al. (2018). Loss of the Martian atmosphere to space: present-day loss rates determined from MAVEN observations and integrated loss through time. *Icarus* 315, 146–157. doi:10.1016/j.icarus.2018.05.030

Jakosky, B. M., and Hallis, L. J. (2024). Fate of an earth-like water inventory on Mars. *J. Geophys. Res. Planets* 129, e2023JE008159. doi:10.1029/2023JE008159

Johnson, R. E., Combi, M. R., Fox, J. L., Ip, W.-H., Leblanc, F., McGrath, M. A., et al. (2008). Exospheres and atmospheric escape. *Space Sci. Rev.* 139, 355–397. doi:10.1007/s11214-008-9415-3

Kasting, J. F. (1988). Runaway and moist greenhouse atmospheres and the evolution of Earth and Venus. *Icarus* 74, 472–494. doi:10.1016/0019-1035(88)90116-9

Kleinboehl, A., Willacy, K., Slipski, M. J., Poncin, P., Halekas, J. S., and Mayyasi, M. (2024). Hydrogen escape on Mars dominated by water vapour photolysis above the hygropause. *Nat. Astron.* 8, 827–837. doi:10.1038/s41550-024-02268-x

Mahaffy, P. R., Webster, C. R., Stern, J. C., Brunner, A. E., Atreya, S. K., Conrad, P. G., et al. (2015). The imprint of atmospheric evolution in the D/H of Hesperian clay minerals on Mars. *Science* 347, 412–414. doi:10.1126/science.1260291

Mayyasi, M., Bhattacharyya, D., Clarke, J., Catalano, A., Benna, M., Mahaffy, P., et al. (2018). Significant space weather impact on the escape of hydrogen from Mars. *Geophys. Res. Lett.* 45, 8844–8852. doi:10.1029/2018gl077727

Mayyasi, M., Clarke, J., Bhattacharyya, D., Chaufray, J. Y., Benna, M., Mahaffy, P., et al. (2019). Seasonal variability of deuterium in the upper atmosphere of Mars. *J. Geophys. Res.* 124, 2152–2164. doi:10.1029/2018JA026244

McElroy, M. B., and Donahue, T. M. (1972). Stability of the martian atmosphere. *Science* 177, 986–988. doi:10.1126/science.177.4053.986

Nagy, A., Kim, J., and Cravens, T. E. (1990). Hot hydrogen and oxygen atoms in the upper atmospheres of Venus and Mars. *Ann. Geophys.* 8, 251–256.

Qin, J., and Waldrop, L. (2016). Non-thermal hydrogen atoms in the terrestrial upper thermosphere. *Nat. Comm.* 7, 13655–655. doi:10.1038/ncomms13655

Ramstad, R., Brain, D. A., Dong, Y., Halekas, J. S., McFadden, J. P., Espley, J., et al. (2022). Energetic neutral atoms near Mars: predicted distributions based on MAVEN measurements. *Astrophys. J.* 927, 11. doi:10.3847/1538-4357/ac4606

Shematovich, V. I. (2013). Suprathermal oxygen and hydrogen atoms in the upper martian atmosphere. *Sol. Syst. Res.* 47, 437–445. doi:10.1134/s0038094613060087

Shematovich, V. I. (2017). Suprathermal oxygen atoms in the Martian upper atmosphere: contribution of the proton and hydrogen atom precipitation. *Sol. Syst. Res.* 51, 249–257. doi:10.1134/S0038094617040050

Shematovich, V. I., and Bisikalo, D. V. (2021). A kinetic model for precipitation of solar wind protons into the Martian atmosphere. *Astron. Rep.* 65, 869–875. doi:10.1134/s106377292110036x

Shematovich, V. I., and Bisikalo, D. V. (2020). Kinetic calculations of the charge exchange efficiency for solar wind protons in the extended martian hydrogen corona. *Astron. Rep.* 64, 863–869. doi:10.1134/S1063772920110074

Shematovich, V. I., Bisikalo, D. V., Diéval, C., Barabash, S., Stenberg, G., Nilsson, H., et al. (2011). Proton and hydrogen atom transport in the Martian upper atmosphere with an induced magnetic field. *J. Geophys. Res.* 116, A11320. doi:10.1029/2011JA017007

Shematovich, V. I., Bisikalo, D. V., Gérard, J.-C., and Hubert, B. (2019). Kinetic Monte Carlo model of the precipitation of high-energy proton and hydrogen atoms into the Martian atmosphere with taking into account the measured magnetic field. *Astron. Rep.* 63, 835–845. doi:10.1134/S1063772919100056

Shematovich, V. I., Bisikalo, D. V., and Zhilkin, A. G. (2021). Effect of variations in the extended hydrogen corona of Mars on the efficiency of charge exchange with solar wind protons. *Astron. Rep.* 65, 203–208. doi:10.1134/S1063772921030033

Shematovich, V. I., and Marov, M.Ya. (2018). Escape of planetary atmospheres: physical processes and numerical models. *Phys. - Uspekhi* 61, 217–246. doi:10.3367/UFNe.2017.09.038212

Tian, F. (2015). Atmospheric escape from solar system terrestrial planets and exoplanets. *Ann. Rev. Earth Plan. Sci.* 43, 459–476. doi:10.1146/annurev-earth-060313-054834

Tian, F., Güdel, M., Johnstone, C. P., Lammer, H., Luger, R., and Odert, P. (2018). Water loss from young planets. *Space Sci. Rev.* 214 (19), 65. doi:10.1007/s11214-018-0490-9

Villanueva, G. L., Mumma, M. J., Novak, R. E., Kaufl, H. U., Hartogh, P., Encrenaz, T., et al. (2015). Strong water isotopic anomalies in the martian atmosphere: probing current and ancient reservoirs. *Science* 348, 218–221. doi:10.1126/science.aaa3630

Wordsworth, R., Kalugina, Y., Lokshtanov, S., Vigasin, A., Ehlmann, B., Head, J., et al. (2017). Transient reducing greenhouse warming on early Mars. *Geophys. Res. Lett.* 44, 665–671. doi:10.1002/2016GL071766

Yelle, R. (2024). Diffusion limited escape of hydrogen from Mars. *Icarus* 418, 116099. doi:10.1016/j.icarus.2024.116099

Zhilkin, A. G., Bisikalo, D. V., and Shematovich, V. I. (2022). Numerical model to study proton polar aurorae on Mars. *Astron. Rep.* 66, 245–254. doi:10.1134/s1063772922030076